Supporting Information

A polyoxometalate-based polymer electrolyte with improved electrode interphase and ion conductivity for high-safety all-solid-state batteries

Xiangfei Yuan,[a] Cui Sun,[a] Jia-Ning Duan,[a] Jingmin Fan,[a] Ruming Yuan,[a] Jiajia Chen,[a] Jeng-Kuei Chang,[b] Mingsen Zheng*[a] and Quanfeng Dong*[a]

[a] State Key Laboratory of Physical Chemistry of Solid Surfaces, Department of Chemistry, College of Chemistry and Chemical Engineering, Collaborative Innovation Center of Chemistry for Energy Materials (*i*ChEM), Xiamen University, Xiamen, Fujian 361005, China

[b] Department of Materials Science and Engineering, National Chiao Tung University, Hsinchu, Taiwan.

*Correspondence: qfdong@xmu.edu.cn, mszheng@xmu.edu.cn

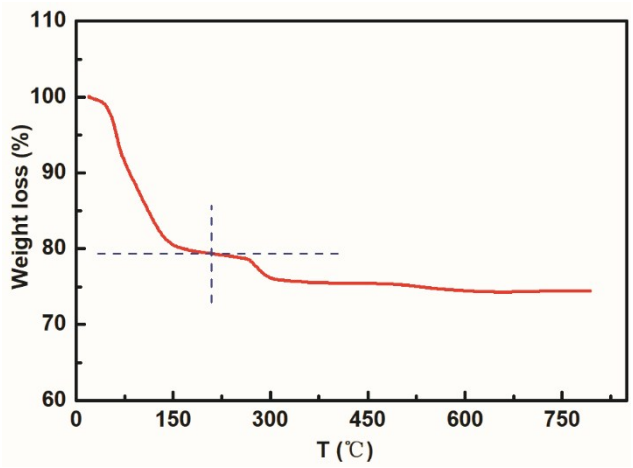

Figure S1. TGA plot of LVC from room temperature to 800 °C.

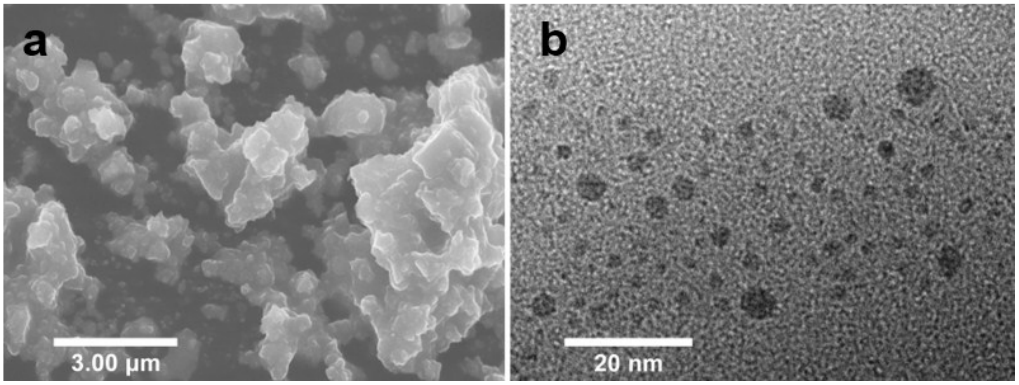

Figure S2. (a) SEM and (b) TEM images of LVC particles.

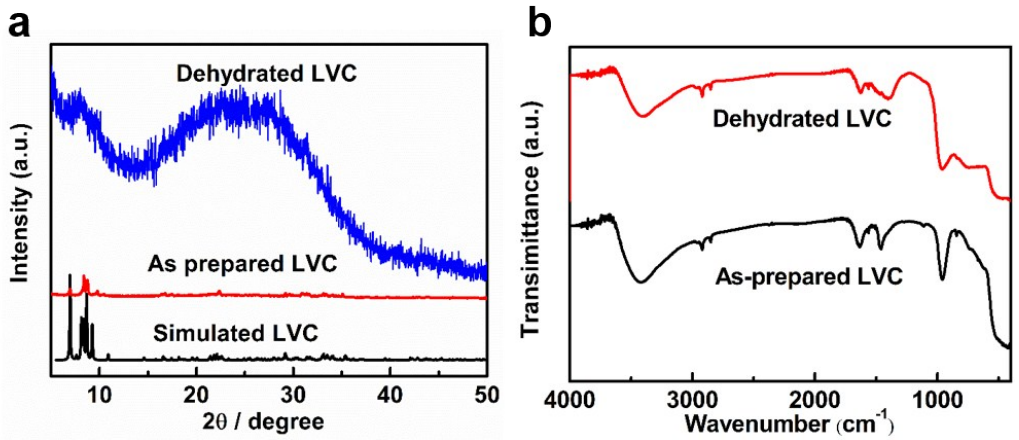

Figure S3. (a) The XRD patterns of as-prepared LVC (red), dehydrated LVC (blue) and simulated (black); (b) FTIR spectroscopy of LVC before (black) and after (red) heating at 200 °C under N_2 for 6 hours.

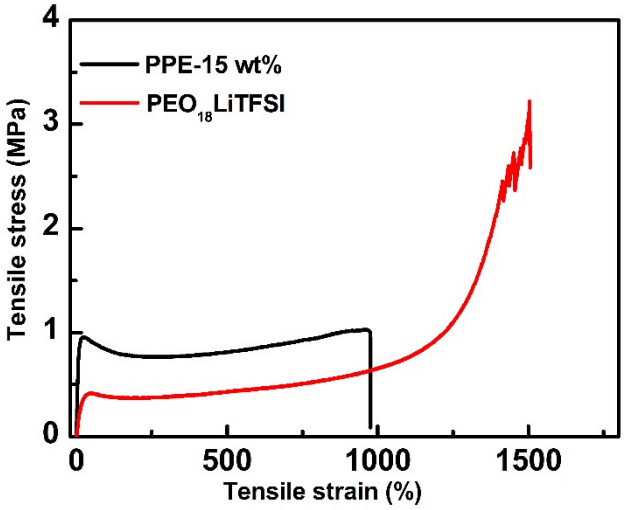

Figure S4. The tensile property of PPEs. Stress-strain curves of PPE-15 wt% (black) and $PEO_{18}LiTFSI$ (red).

Table S1. The tensile stress, tensile strain and Young's modulus of PPEs.

Solid electrolytes	Tensile stress (MPa)	Tensile strain (%)	Young's modulus (MPa)
PPE-15wt%	0.96	974.93	4.57
$PEO_{18}LiTFSI$	0.41	1506.30	1.50

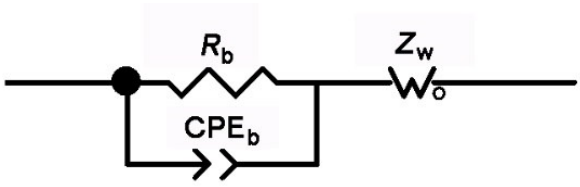

Figure S5. Equivalent circuit for the PPE membranes.

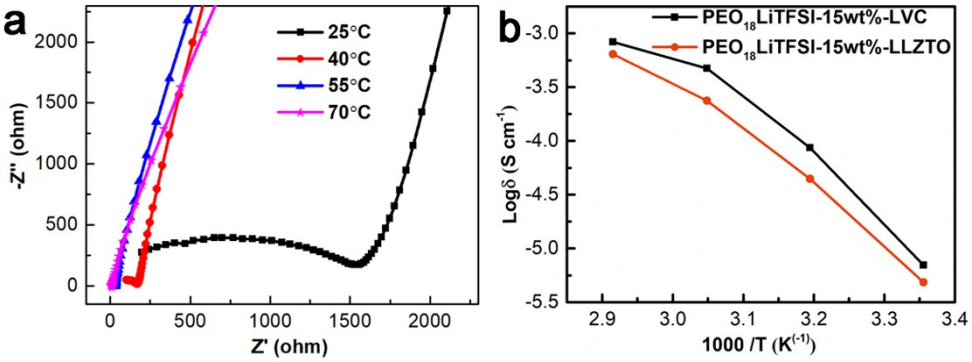

Figure S6. (a) Nyquist plots of PEO_{18}LiTFSI-15 wt%-LLZTO comprised of the same proportion among PEO, LiTFSI and LLZTO (d=2 μm) as PPE-15 wt% at temperatures from 25 °C to 70 °C; (b) Arrhenius plots for the ionic conductivity of composite polymer solid electrolyte with different LVC and LLZTO loading amounts.

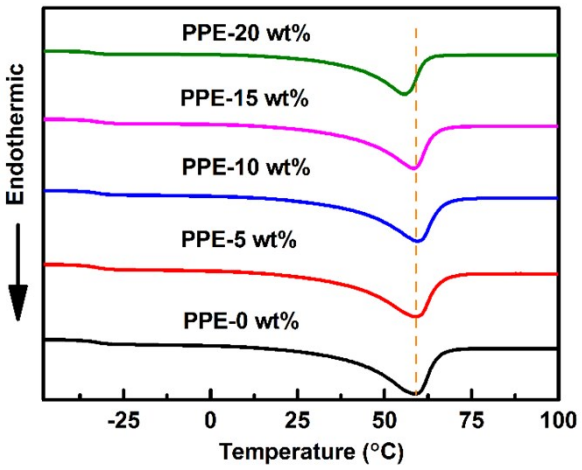

Figure S7. DSC characterization of PPEs with different LVC contents.

Table S2. Comparison of the T_g, T_m, ΔH_c and χ_c of PPEs with different LVC contents.

Sample	T_g (°C)	T_m (°C)	ΔH_c ($J \cdot g^{-1}$)	χ_c (%)
PEO_{18}LiTFSI	-32.7	58.9	72.62	33.98
PPE-5 wt%	-33.6	59.1	67.82	31.74
PPE-10 wt%	-34.1	59. 5	64.24	30.06
PPE-15 wt%	-34.5	58.4	60.97	28.53
PPE-20 wt%	-34.9	55.7	51.26	23.99

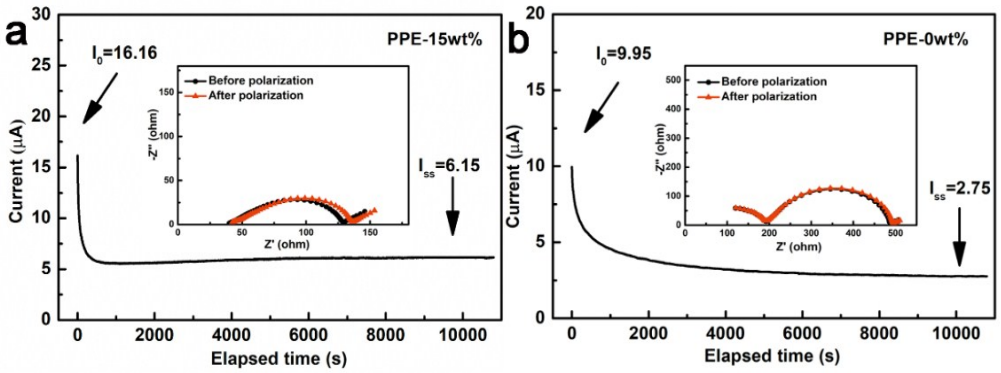

Figure S8. Chronoamperometry-time curves during the polarization of (a) Li| PPE-15 wt% |Li; (b) Li| PPE-0 wt% |Li cell at 40 °C, followed an applied potential of 5 mV; Insert: corresponding nyquist spectra before and after polarization.

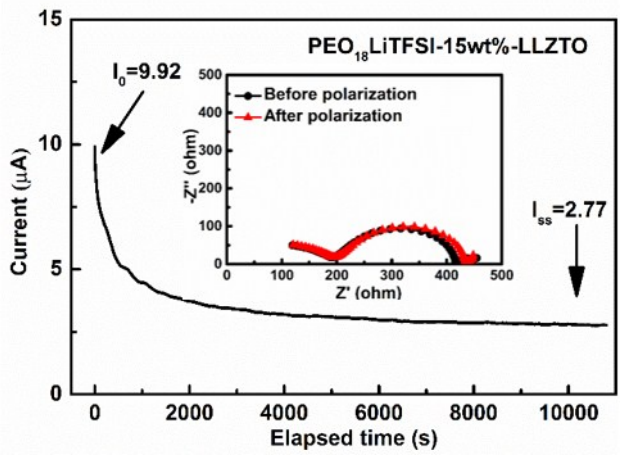

Figure S9. Chronoamperometry-time curves during the polarization of Li| PEO_{18}LiTFSI-15 wt%-LLZTO |Li cell at 40 ^{o}C, followed an applied potential of 5 mV; Insert: corresponding nyquist spectra before and after polarization.

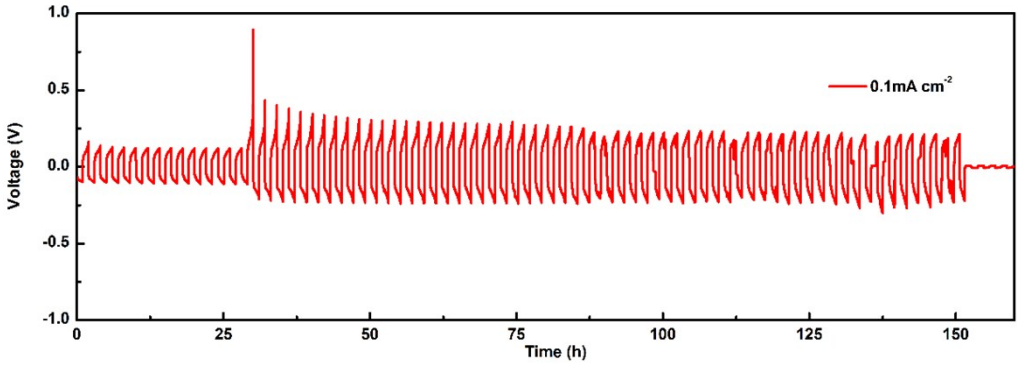

Figure S10. Voltage profile during the lithium plating/striping cycling in Li-Li symmetrical cell with routine PEO_{18}LiTFSI electrolytes with a current density of 0.10 mA cm^{-2} at 40 ^{o}C.

Table S3. Comparison of our work with related studies about the lithium plating/striping measurement in Li-Li symmetrical cell.

Solid electrolytes	Current density and temperature for Li deposition/stripping	Overpotential for Li deposition/stripping (mV)	Cycling hours for Li deposition/stripping (h)	Ref
PPE-15wt%	0.10 mA cm^{-2} at 40 ^{o}C	18	>1300	This work
APCE-300 K	0.10 mA cm^{-2} at 60 ^{o}C	~30	> 80	Nano Lett., 2018, **18**, 3829-3838.
LPD@PVDF SIPE	0.50 mA cm^{-2} at 25 ^{o}C	33	>1050	Small, 2018, **14**, 1801420
PEO-LLZTO-PEG-60 wt% LiTFSI composite electrolyte	0.50 mA cm^{-2} at 55 ^{o}C	~40	>680	Nano Energy, 2018, **46**, 176-184.
P@CMOF	0.10 mA cm^{-2} at 60 ^{o}C	70	400	Energy Storage Mater, 2019, **18**, 59-67.
PEO-50 wt % LATP composite solid electrolyte	0.1 mA cm^{-2} at 60 °C	30	200	J. Phys. Chem. C 2018, **122**, 9852−9858
$Li_{6.1}Ga_{0.3}La_3Zr_2O_{12}$ and NASICON-type Li_2O-Al_2O_3-P_2O_5-TiO_2-GeO_2 (LATP) pellets	0.10 mA cm^{-2} at room temperature	< 50	>220	Energy Environ. Sci, 2018, **11**, 1803-1810.

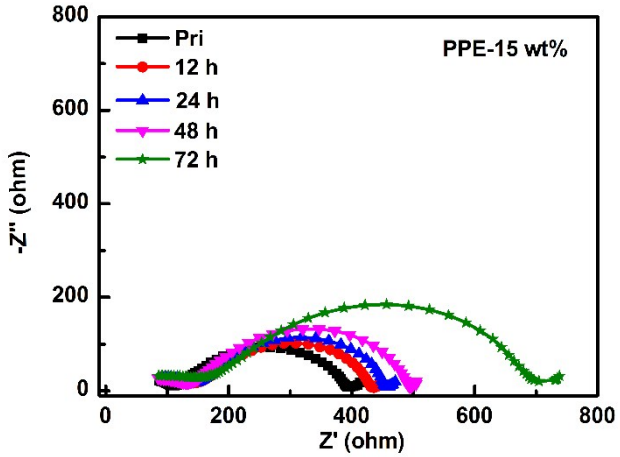

Figure S11. The impedance spectra of Li|PPE-15 wt%|Li cell bias voltage 0.18 V for different time at 40 °C.

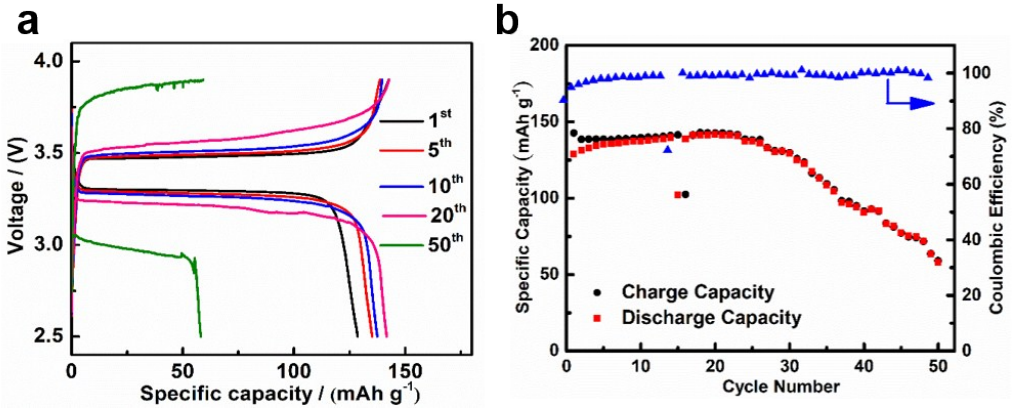

Figure S12. The typical cycling performance of $LiFePO_4$| $PEO_{18}LiTFSI$ |Li cells. (a) Voltage profile and (b) cycling performance at 0.1 C at 40 °C.

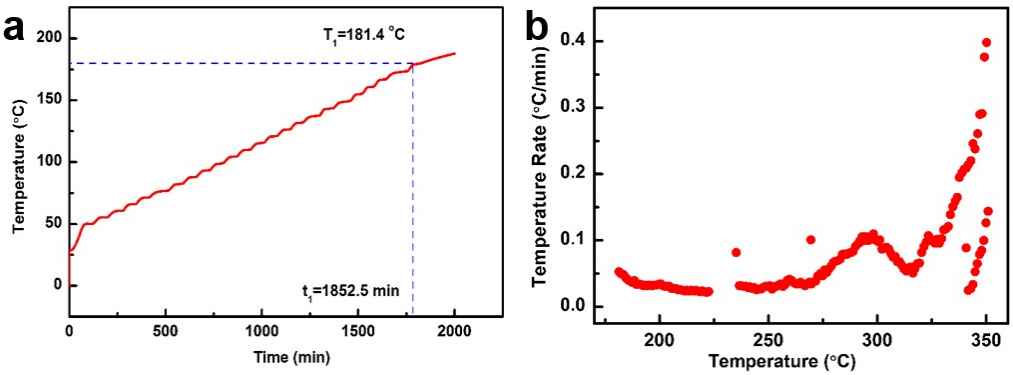

Figure S13. (a) A corresponding enlargement of ARC exotherm with $LiFePO_4$| PPE-15 wt% |C cell; (b) The scatter diagram of corresponding temperature rate variation.

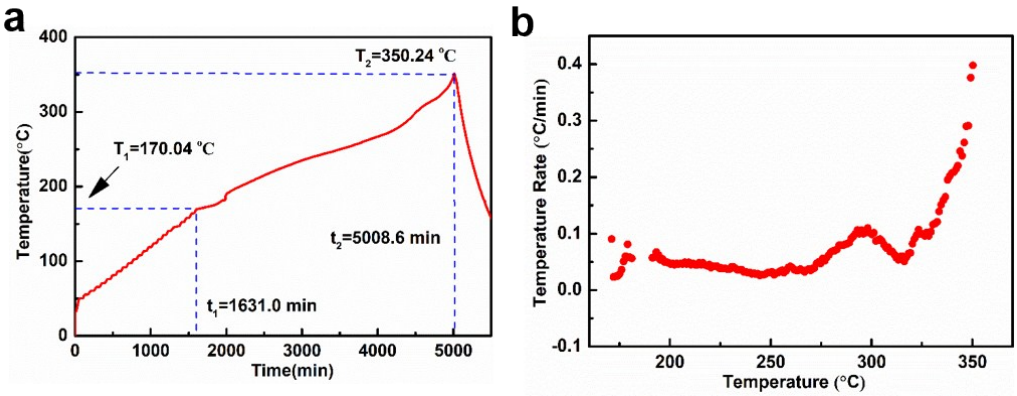

Figure S14. (a) ARC exotherm of $LiFePO_4$| PPE-15 wt% |Li cell ranging from 50 °C to 360 °C.; (b) The scatter diagram of corresponding temperature rate variation.

Table S4. Comparison of ARC data between $LiFePO_4$| PPE-15wt%|C and $LiFePO_4$| PPE-15wt%|Li cells during the self-heating process.

Batteries based-on PPE	Onset Temperature (°C)	Onset Temperature Rate(°C min^{-1})	Max Rate Temperature(°C)	Max Temperature Rate(°C min^{-1})
$LiFePO_4$| PPE-15wt%|C	181.4	0.039	351.0	0.398
$LiFePO_4$| PPE-15wt%|Li	170.04	0.09	350.2	0.398